Earth and Planetary Science Letters 559 (2021) 116808

Contents lists available at ScienceDirect

Earth and Planetary Science Letters

www.elsevier.com/locate/epsl

The relative behaviour of bulk and shear modulus as an indicator of the iron spin transition in the lower mantle

B.L.N. Kennett

Research School of Earth Sciences, The Australian National University, Canberra ACT 2601, Australia

ARTICLE INFO

Article history:
Received 22 July 2020
Received in revised form 1 February 2021
Accepted 4 February 2021
Available online 9 February 2021
Editor: J. Badro

Keywords:
spin transition
Earth models
bulk modulus
shear modulus
deep Earth

ABSTRACT

For a regular material, in a single state, the effect of increasing pressure is to produce a linear relation between shear modulus (G), bulk modulus (K) and pressure (p). Such a dependence on pressure fits the behaviour of individual mineral and mineral composites well. For the iron bearing minerals in the lower mantle, the transition from the high-spin state to the low-spin state with increasing pressure produces deviations from this simple behaviour, due to a much larger reduction of the bulk modulus than the shear modulus in the spin crossover. There are linear zones in the dependence of the modulus ratio G/K on pressure scaled by bulk modulus (p/K) above and below the transition, with a complex excursion to high ratios in between. With increasing temperature the spin transition is smoothed out in depth, and is expected to be smooth along a mantle geotherm. For the *ak135* body-wave model of radial Earth structure there is a slight, but distinct, change of slope in the relation between the modulus ratio and scaled pressure corresponding to a depth range around 1550 km. This feature is strongly suggestive of a residual effect of a 3-D averaged spin transition in the ferropericlase component of the lower mantle.

1. Introduction

The iron bearing minerals of the lower mantle undergo spin transitions with increasing pressure that modify their physical parameters. Two major review papers (Lin et al., 2013; Badro, 2014) have presented full accounts of the development of the concept together with the experimental and computational evidence for significant modification of elastic moduli (particularly bulk modulus) and thermal conductivity. At shallow depths, mantle minerals contain iron in the high-spin electronic state. The effect of pressure enhances the splitting energy between the orbitals in the iron atoms and so favours the low-spin state. Thus, with increasing pressure, the configurations of the outermost shell electrons in iron atoms are modified and produce an electronic spin-pairing transition from a high-spin to a low-spin state. Under the temperature conditions in the lower mantle the spin crossover transition is expected to be gradual and occur over a broad span of pressures.

For ferropericlase the spin transition is associated with ferrous iron (Fe^{2+}). At mantle temperatures the spin crossover is generally considered to occur in the pressure range 50–90 GPa, though the exact range is still a matter of debate (e.g., Tsuchiya et al., 2006; Lin et al., 2007; Mao et al., 2011; Holmström and Stixrude, 2015). The transition is accompanied by a reduction in the bulk modulus with much less effect on the shear modulus and density (e.g., Marquardt et al., 2009; Wentzcovitch et al., 2009). The size of such spin-transition effects is still not entirely clear, with conflicting reports from different experimental and computational studies (Crowhurst et al., 2008; Wentzcovitch et al., 2009; Antonangeli et al., 2011; Wu et al., 2013; Shukla et al., 2016; Marquardt et al., 2018). The spin transition shifts to higher pressures with increasing iron content (e.g., Speziale et al., 2005).

In bridgmanite the situation is more complex, with the potential for different transitions depending on the valence of iron and its position in the silicate lattice structure (Badro, 2014). The net effect on elastic properties appears to be small (Caracas et al., 2010), and Shukla et al. (2016) have demonstrated that the presence of aluminium can suppress the effects of the spin transition.

The preference of iron for the low-spin state tends to drive iron partitioning, so that bridgmanite at high pressures is expected to be enriched in ferric iron (e.g. Badro, 2014), whilst ferropericlase retains ferrous iron. The effect of the spin crossover is therefore expected to produce some change in the Fe-Mg partitioning between bridgmanite and ferropericlase (Irifune et al., 2010; Piet et al., 2016).

Houser et al. (2020) have made a detailed study of the effects of temperature and composition on the spin transition in the iron bearing minerals in the context of looking at discriminants between different potential compositions for the lower mantle. They note that the effect of the spin transition in ferropericlase

E-mail address: Brian.Kennett@anu.edu.au.

https://doi.org/10.1016/j.epsl.2021.116808
0012-821X/

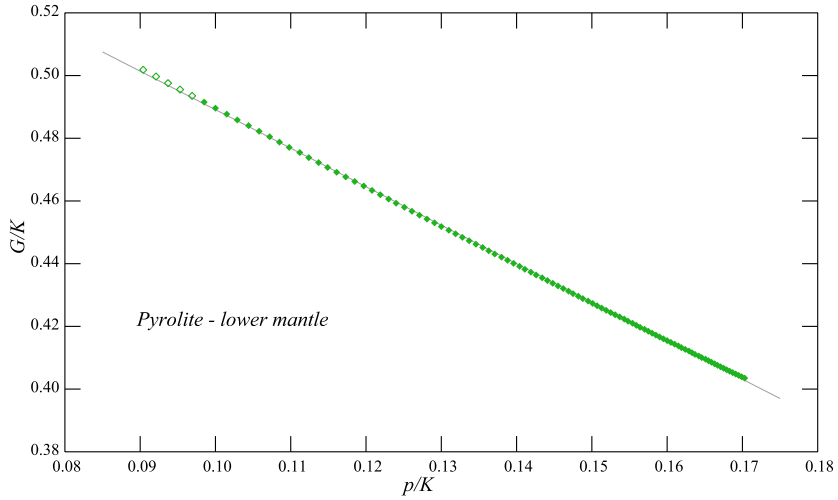

Fig. 1. Illustration of the linear dependence of G/K on p/K for a pyrolitic composition mineral assemblage for the lower mantle from Gréaux et al. (2019). No spin effects are included. The open symbols indicate the zone where some residual garnet may be present. Pressure range 27–126 GPa.

could provide a means of distinguishing between relatively ferromagnesian and silica-rich compositions.

Despite the expectation of noticeable changes in physical properties due to the presence of the spin transition, seismological manifestations have been lacking. Comparisons have tended to be made with the *PREM* reference model (Dziewonski and Anderson, 1981), where a single cubic polynomial spans the entire lower mantle for seismic velocities and density and so localised effects would be suppressed. The more flexible parametrisation employed in the *ak135* model also shows no direct indication of spin transition effects. The P wavespeeds and S wavespeeds for *ak135* are self-consistent (Cammarano et al., 2010; Kennett, 2020a), but show a slightly different trend for epicentral distances beyond 60°, compared to shorter distances.

Comparison with an individual wavespeed or modulus are not sufficient to identify subtle effects, but the ratio of shear to bulk modulus G/K as a function of pressure scaled by bulk modulus p/K is a sensitive indicator of variations in material behaviour. For a regular material with no phase transitions, the modulus ratio depends linearly on scaled pressure. The presence of a second-order phase transition, such as the spin crossover, modifies the pattern with distinct linear segments on either side of the transition and a complex intermediate behaviour. Body wave models of the radial structure of the lower mantle indicate a change in the slope of the modulus ratio as a function of normalised pressure that is compatible with weak averaged effects of the spin transitions.

Valencia-Cardona et al. (2017) have proposed the use of Bullen's parameter as an indicator of the spin transition, since this measure of departures from adiabacity incorporates the bulk modulus. However estimation of this parameter requires density gradients, which are much less well constrained than other seismic parameters (e.g. Kennett, 1998).

2. Comparing bulk and shear moduli

For a material in a single state the relation between the shear modulus G, bulk modulus K and pressure p is well approximated by

$$G = aK - bp. \tag{1}$$

An equivalent form to (1) was derived by Falzone and Stacey (1980) from a model with a purely central potential function between atoms, with changes in bond lengths in a deformed crystal calculated to second-order in strain. The relation (1) is consistent with the interactions of stretching and bending contributions to material deformation under pressure, and is satisfied by experimental results on many different classes of minerals (e.g. Kennett, 2020b). Burakovsky et al. (2004) have pointed out that the coefficients a and b in equation (1) can be specified in terms of the notional initial values of the shear and bulk moduli (G_0, K_0) and their pressure derivatives (G_0', K_0'), regardless of whether that state can actually be achieved. The linear relation can be expressed as

$$\frac{G}{K} = \left(\frac{G_0}{K_0}\right) - \left[\left(\frac{G_0}{K_0}\right)K_0' - G_0'\right]\frac{p}{K}. \tag{2}$$

The ratio G/K can be derived from seismic wavespeeds without the influence of density ρ. $G/K = \beta^2/\phi^2$ in terms of bulk-sound speed ϕ and S wavespeed β, where $\phi^2 = \alpha^2 - 4\beta^2/3$ and α^2 is the P wavespeed. The scaled pressure p/K is also only mildly affected by changes in the density distribution with depth. Kennett (2017, 2020b) has used (1), (2) to link a representation of shear properties to existing equations of state for pressure and bulk modulus.

The linear relation (2) between the ratio of moduli and scaled pressure also provides a good description of the properties of mineral assemblages. In Fig. 1 we illustrate the results for a pyrolytic model for the Earth's lower mantle developed by Gréaux et al. (2019). The dominant minerals are bridgmanite and ferropericlase, included without any allowance for spin transitions. Some residual majorite garnet is present at the top of the lower mantle, marked by open symbols, and this leads to a slight deviation from the overall linear trend.

When a material changes state, the intercept and slope of the G/K vs p/K relation will be modified and so deviations will be introduced from the linear relation (2) for the original configuration. As we shall see in the next section, the spin crossover in the iron content of lower mantle minerals produces marked deviations from the linear trend.

3. Effects of spin transitions

Many studies of the spin transition have concentrated on the effects on bulk modulus as a function of temperature and pressure (e.g., Marquardt et al., 2018; Liu et al., 2018), but a clearer picture emerges when the relative behaviour of the shear and bulk modulus, or the corresponding wave speeds, are considered (e.g. Marquardt et al., 2009; Wu et al., 2013; Wu and Wentzcovitch, 2014; Wu, 2016; Wu and Wentzcovitch, 2017; Marquardt and Thomson,

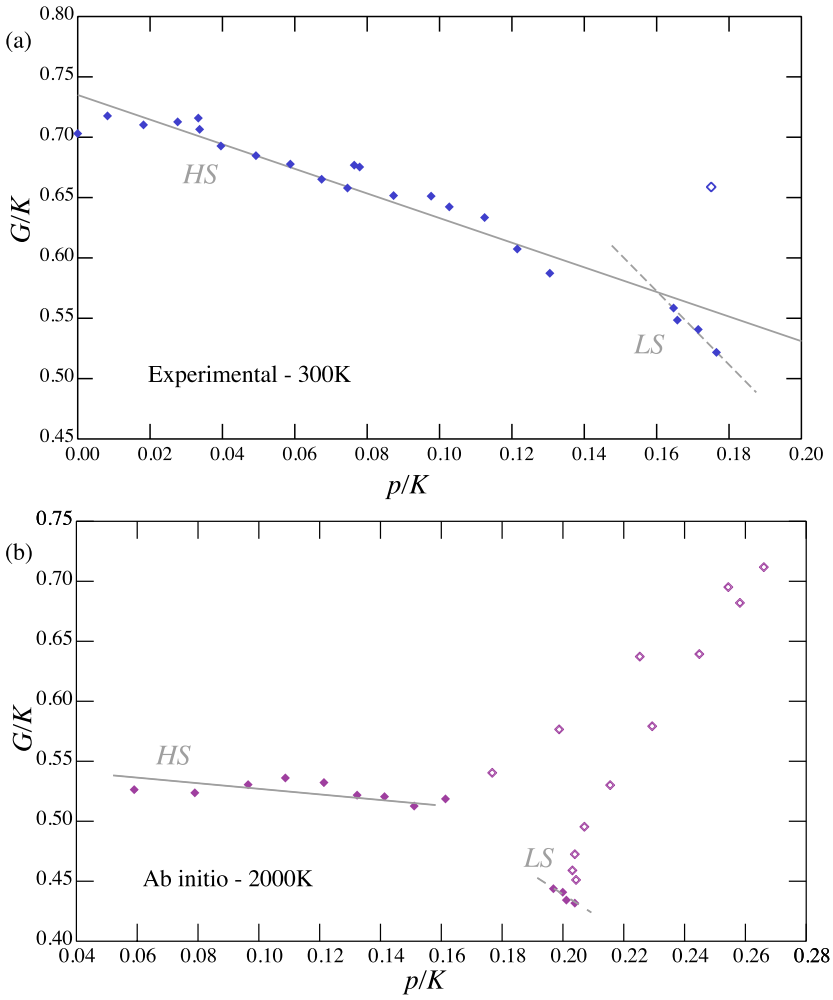

Fig. 2. Plots of the relation of G/K to p/K for ferropericlase. Both the high-spin state at lower pressures (*HS*) and the low-spin state at high pressures (*LS*) show approximately linear relations, but with different slope. In the transition region this pattern is disrupted by the reduction of the bulk modulus, as indicated by the results shown with an open symbol. (a) Experimental results of Marquardt et al. (2009) for single-crystal $Mg_{0.9}Fe_{0.1}O$ crossing the spin transition in ferropericlase at room temperature. Pressure range 27–126 GPa. (b) Ab initio results from Wu et al. (2013) at 2000 K for $Mg_{0.8125}Fe_{0.1875}O$ displaying the full pattern of the excursion in the moduli ratio across the spin transition. Pressure range 10–140 GPa.

2020). An alternative is to use Poisson's ratio (Fu et al., 2018) that can also be expressed as a function of the modulus ratio G/K.

We here illustrate the effect of the presence of a spin transition through the pressure dependence of the modulus ratio G/K with results from both experimental work and ab initio calculations that have estimated both bulk and shear moduli as a function of pressure. We present results for both ferropericlase (Fig. 2) and iron-bearing bridgmanite (Fig. 3).

In Fig. 2(a), we display the behaviour of the modulus ratio G/K as a function of scaled pressure p/K for single-crystal $(Mg_{0.9}Fe_{0.1})O$ from the experimental results of Marquardt et al. (2009). For this ferropericlase study, at room temperature, there is a marked change in the slope of the G/K relation between the low pressure high-spin state (HS) and the higher pressure low-spin state (LS). The reduction in the bulk modulus through the spin crossover is so large that most points in this zone lie well off the plot to the right. The behaviour is similar to that found for the ab initio calculations of Wu et al. (2013) shown in Fig. 2(b). Here results at a constant temperature of 2000 K are displayed. The excursion in the modulus ratio associated with the spin transition is much larger at lower temperatures. The softening of the bulk-modulus through the spin crossover for ferropericlase has been demonstrated at seismic frequencies by Marquardt et al. (2018), but no associated shear modulus results were reported.

In Fig. 3 we show equivalent results for bridgmanite from the experimental study of Fu et al. (2018) at room temperature, and ab initio results from Shukla et al. (2016) at 1200 K for several different compositions. The experimental results with the presence of ferric iron show a pronounced spin transition. In contrast the ab initio calculations indicate suppression of the spin transition in the presence of Al irrespective of the presence of ferric iron, for all temperatures.

The examples we have displayed for ferropericlase and bridgmanite demonstrate the behaviour of the modulus ratio G/K with scaled pressure p/K at constant temperature. However, the spin transition is strongly temperature dependent, broadening with increasing temperature. Shukla et al. (2016) have carried out a suite of ab initio computations for various modifications of bridgmanite, and present results for paths along the mantle geotherm of Boehler (2000). In Fig. 4(a) we display the G/K vs p/K behaviour on the lower mantle geotherm for this set of materials, which range from pure $MgSiO_3$ bridgmanite, to iron substitution on both magnesium and silicon sites [Fe3+]Mg-[Fe3+]Si. This last material displays a distinct spin transition that manifests as a smoothly varying curve in Fig. 4 that deviates noticeably from the trend with aluminium substitution on silicon sites, for which the spin transition is suppressed. Hence, in the presence of a lower mantle spin transition we would expect to see two approximately linear segments in G/K

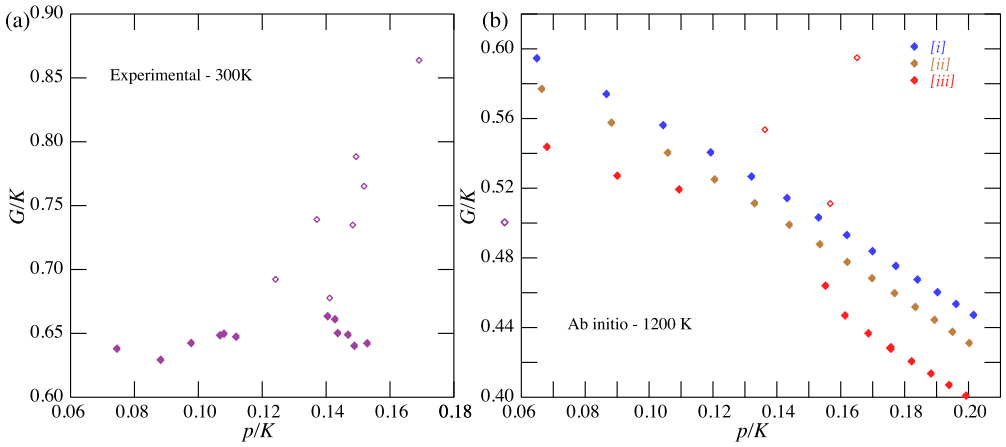

Fig. 3. Plots of the relation of G/K to p/K for bridgmanite, results in the spin transition region are shown with open symbols. (a) Experimental results of Fu et al. (2018) at room temperature for the iron-bearing composition $Mg_{0.96}Fe^{2+}_{0.036}Fe^{3+}_{0.014}Si_{0.99}O_3$. Pressure range 24–69 GPa. (b) Ab initio results at 1200 K from Shukla et al. (2016) for different compositions (i) $(Mg_{0.875}Al_{0.125})(Si_{0.875}Al_{0.125})O_3$, (ii) $(Mg_{0.875}Fe^{3+}_{0.125})(Si_{0.875}Al_{0.125}))O_3$, (iii) $(Mg_{0.875}Fe^{3+}_{0.125})(Si_{0.875}Fe^{3+}_{0.125})O_3$. Only the variant (iii) with no Al displays a spin transition. Pressure range 20–150 GPa.

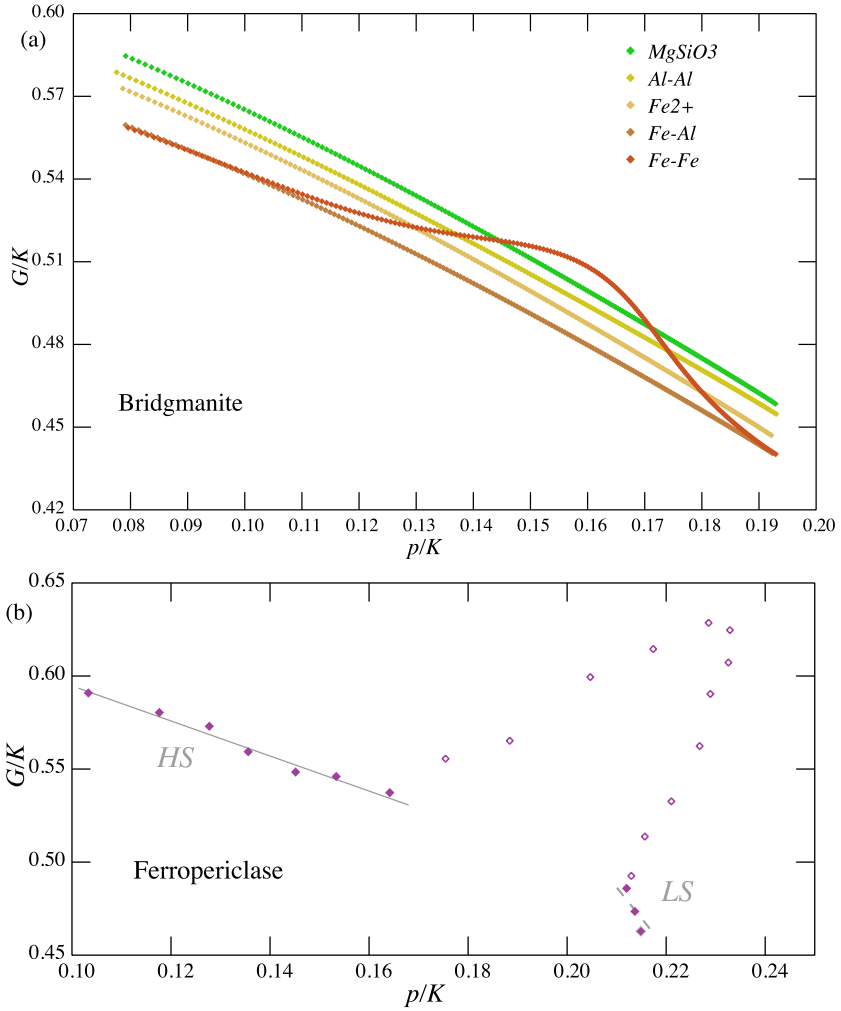

Fig. 4. (a) Plot of G/K vs p/K for the ab initio computational results of Shukla et al. (2016) on modifications of bridgmanite, indicated by simplified codes. The calculations were made along the lower mantle geotherm of Boehler (2000) for pure $MgSiO_3$ bridgmanite (*MgSiO3*), and various substitutions in $MgSiO_3$ bridgmanite:
(*Al-Al*) [Al]Mg-[Al]Si – 5% Al, (*Fe2+*) $[Fe^{2+}]$Mg – 10% Fe^{2+}, (*Fe-Al*) $[Fe^{3+}]$Mg-[Al]Si – 10% Fe^{3+}, Al, and (*Fe-Fe*) [Fe3+]Mg-[Fe3+]Si – 5% Fe^{3+}. Pressure range 24–150 GPa. The spin crossover in the presence of ferric iron has a strong effect on the behaviour.
(b)Plot of G/K vs p/K for the ab initio computational results of Wu et al. (2013) for ferropericlase $Mg_{0.875}Fe_{0.125}O$, along the lower mantle geotherm of Brown and Shankland (1981). Results in the spin transition region are shown with open symbols. Pressure range 25–130 GPa.

vs P/K at low and high pressures, but neither slope would reflect the constitutive state of bridgmanites without a significant spin crossover effect.

Although the effects of the spin transition in bridgmanite along a mantle geotherm are muted, there are still considerable reductions in bulk modulus for ferropericlase. In Fig. 4(b) we display the ab initio results of Wu et al. (2013) for ferropericlase along the mantle geotherm of Brown and Shankland (1981). A very noticeable excursion in G/K associated with the spin transition is present between the high-spin and low-spin states. This excursion becomes even larger if the proportion of Fe is increased (Wu et al., 2013). Thus the spin transition in ferropericlase in the lower mantle can be expected to make a significant effect on the seismic properties of any aggregate in which it is present.

4. Lower mantle seismic models

The dominant variation of the material properties of the Earth is with depth, but three-dimensional variations are significant in the upper part of the mantle and near the core-mantle boundary for both compressional and shear waves (e.g. Saltzer et al., 2001; Kennett and Gorbatov, 2004; Simmons et al., 2010). Seismological models for the radial variation of elastic parameters represent averaging of the three-dimensional Earth and its temperature and compositional variations.

The *PREM* model of Dziewonski and Anderson (1981) was primarily constructed from the centre frequencies of the free oscillations of the Earth, with additional constraints from the travel times of seismic body waves. For the lower mantle, the primary constraint is on shear wavespeed and control on the *P* wavespeed is weaker. The normal modes provide direct control on the spherical averaged model as a function of depth. In the *PREM* model, a single cubic function of radius is specified from 770 km to 2740 km for both *P* and *S* wavespeeds as well as density ρ. This parametric representation cannot adapt to any localised features, and so even if spin effects were present in a limited depth range they would have little influence on the overall distribution of properties in the lower mantle.

In contrast, models constructed from body-wave observations, such as *ak135* (Kennett et al., 1995) have independent constraints on *P* and *S* wavespeeds. An associated density distribution was created by Montagner and Kennett (1996), by fitting normal mode frequencies. The *ak135* model is specified by control points in radius with linear interpolation between, but since the starting point was parametric some influence can remain (Kennett, 2020a). The travel time observations used to construct the body-wave models average three-dimensional structure to provide travel time curves as a function of epicentral distance. Many different seismic phases were used in the construction of the *ak135* model, and the resulting model represents an approximation to a radial average, but with likely bias from the uneven distribution of seismic stations and earthquakes across the globe.

Because model *ak135* was developed to provide a representation of travel times, an implicit assumption was made that the seismic wavespeeds would show a monotonic increase with depth through the mantle. Thus no allowance was made for possible localised reductions in *P* and *S* wavespeeds.

Although the *ak135* model has proved very effective and is in use as the primary model for earthquake location by international agencies, more recent observations from the differential times of *SmKS* phases that have multiple reflections on the underside of the core-mantle boundary (e.g. Kaneshima and Helffrich, 2013) have indicated the need for slight adjustments to the structure at the top of the core. Modifications to one part of the model require compensating adjustments elsewhere to maintain a fit to the full suite of seismic phases. Kennett (2020a) has developed a modified model *ek137* to match the full range of *SmKS* observations. This model includes some slight changes to the lower mantle from *ak135*, notably for *S* in the lowermost mantle, as well as adjustments at the top of the core. The model *ek137* was constructed starting from *ak135* and shares the characteristic of monotonic increase in wavespeeds through the lower mantle.

The constraints on the distribution of density with depth are weaker than for the seismic wavespeeds, and are principally controlled by the properties of low frequency normal modes in conjunction with the mass and moment of inertia of the Earth. The available data are compatible with a nearly adiabatic distribution, but do not require such a property (Kennett, 1998). This is why it is desirable to look at aspects of Earth structure that minimise dependency on the specifics of the density distribution.

For each of the seismological models we can extract the shear and bulk moduli, and construct the pressure distribution with depth. The resulting patterns of dependence of the elastic modulus ratio G/K on the scaled pressure p/K are displayed in Fig. 5. For all the seismological models the dependence is not far from linear, but for the body wave models *ak135*, *ek137* there is a slight, but distinct, change of slope with increasing scaled pressure. These trends are indicated in Fig. 5 by light grey lines fitted to the low- and high-pressure behaviour. The zone between $p/K = 0.13$ and $p/K = 0.156$ shows a different slope to that for the shallower and deeper parts of the lower mantle. This cross-over zone corresponds to the depth range from 1300–1750 km. The change in slope with scaled pressure is suggestive of the features seen in the spin transition results in the previous section.

Because the body-wave seismic models were constructed with a monotonic increase in seismic wavespeeds, locally reduced wavespeeds are not allowed and so there can be no equivalent of the excursion in G/K linked to such a reduction, as in Fig. 4(b) for ferropericlase. The change in slope in the G/K vs p/K behaviour for models *ak135* and *ek137* is compatible with the presence of a weak residual effect from a spin transition, spread over a pressure range of around 25 Pa. The change in slope would be associated with the spin crossover in ferropericlase rather than bridgmanite.

The slight, but distinct, change in slope in the modulus ratio as a function of scaled pressure is indicative of a change of state in the lower mantle. This change is likely to be linked to a muted signal of the iron spin transition. A change in the gradients of the seismic wavespeeds between the shallower and deeper parts of the lower mantle has been noted by Cobden et al. (2009) with the transition most prominent in the range 1300-1700 km. A variety of thermal and thermo-chemical scenarios were assessed by Cobden et al. (2009), but none were wholly satisfactory. A spin transition explanation was dismissed because of the steady increase in seismic wavespeed with depth in the seismic models derived from body-wave observations. However, as we have noted above, the monotonic increase is an intrinsic feature of the models and cannot be used for discrimination of the physical state.

5. Discussion and conclusions

Distinct changes in properties occur between the shallower and deeper parts of the lower mantle in radial Earth models, with a transition where the spin transitions are expected. Such 1-D earth models represent an average of three-dimensional structure modulated by the way that the seismic probes have sampled the Earth. The variations of the modulus ratio $R_m = G/K$ can be represented, to first order, as a combination of those for the bulk-sound speed ϕ and the shear wavespeed β, since $R_m = \beta^2/\phi^2$,

$$\frac{\delta R_m}{R_m} \approx 2\frac{\delta\beta}{\beta} - 2\frac{\delta\phi}{\phi}. \tag{3}$$

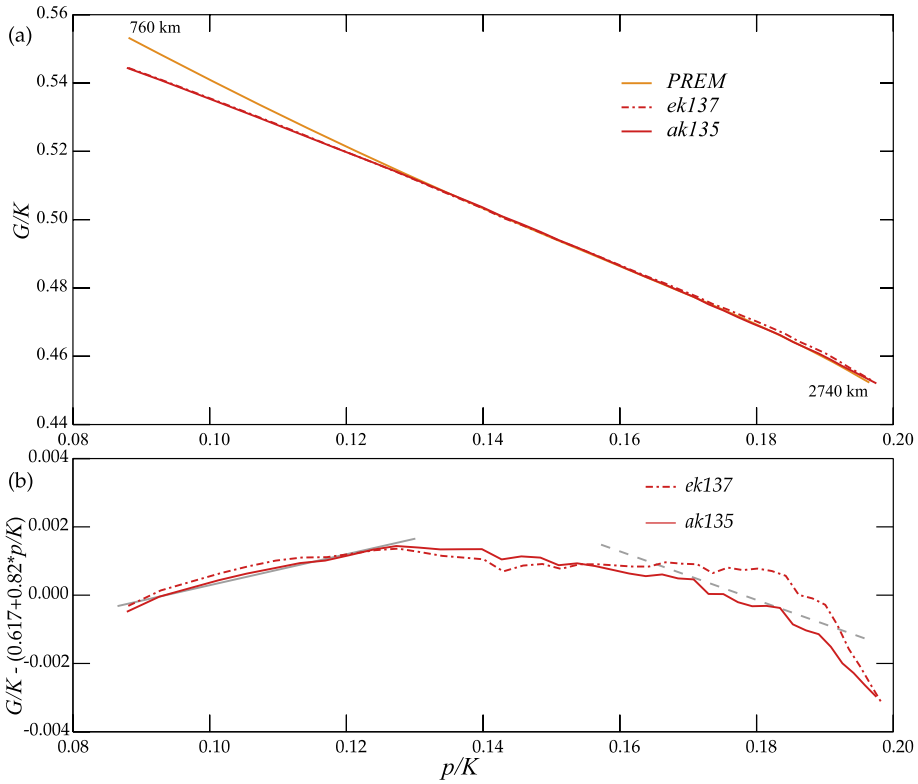

Fig. 5. (a) Plot of G/K vs p/K for seismological models of the lower mantle: *PREM* – Dziewonski and Anderson (1981) from normal modes; *ak135* – Kennett et al. (1995) and *ek137* – Kennett (2020a) from body-wave observations. Pressure range 27-126 GPa. (b) More detailed plot with removal of the main trends in the G/K vs p/K behaviour. Light grey guiding lines indicate the differences in the low- and high-pressure slopes for the body-wave models *ak135*, *ek137*.

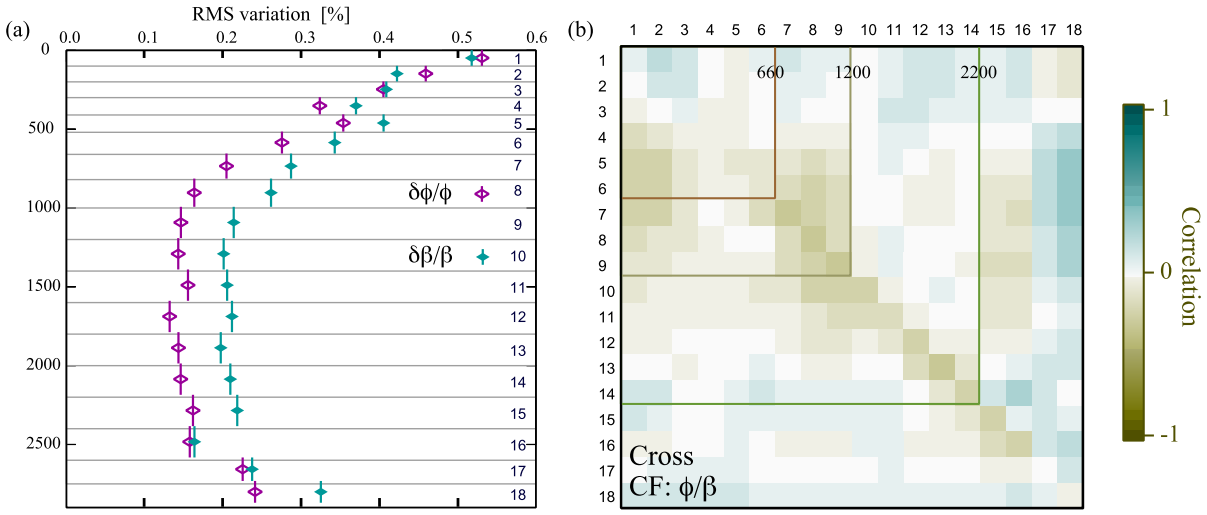

Fig. 6. (a) Relative variations of bulk-sound speed ($\delta\phi/\phi$) and shear wavespeed ($\delta\beta/\beta$) from *ak135* as a function of depth for the 18-layer joint tomographic model of Kennett and Gorbatov (2004). (b) Radial cross-correlation of the bulk-sound speed and shear wavespeed variations as a function of layer number. Note that the shear resolution at the base of the mantle is limited by the cross-over with *SKS*, and this affects the amplitude of variations, e.g., in layer 16. (For interpretation of the colours in the figure(s), the reader is referred to the web version of this article.)

We can therefore make use of the global tomographic models for ϕ and β of Kennett and Gorbatov (2004) derived by joint inversion of *P* and *S* travel times for events which recorded both *P* and *S*, so model sampling and resolution are directly comparable for the two wavespeed distributions.

In Fig. 6(a) we show the rms variations for both bulk-sound speed and shear wavespeed, compared with the *ak135* reference model, as a function of depth in the 18-layer model of Kennett and Gorbatov (2004). The amplitude of the variations connected to the bulk-sound speed reach a minimum in the mid-mantle where spin effects should be most prominent. The size of such variations can be suppressed by anti-correlation of bulk modulus and density variations (Valencia-Cardona et al., 2017), but a similar effect would occur for shear wavespeed variations. The relative variations in the modulus ratio would still be least in the mid-mantle. There is weak anti-correlation in the variations of bulk-sound speed and shear wavespeed through the lower mantle in the joint-tomography model as illustrated in Fig. 6(b). Wu (2016) has shown that the presence of a spin transition in ferropericlase

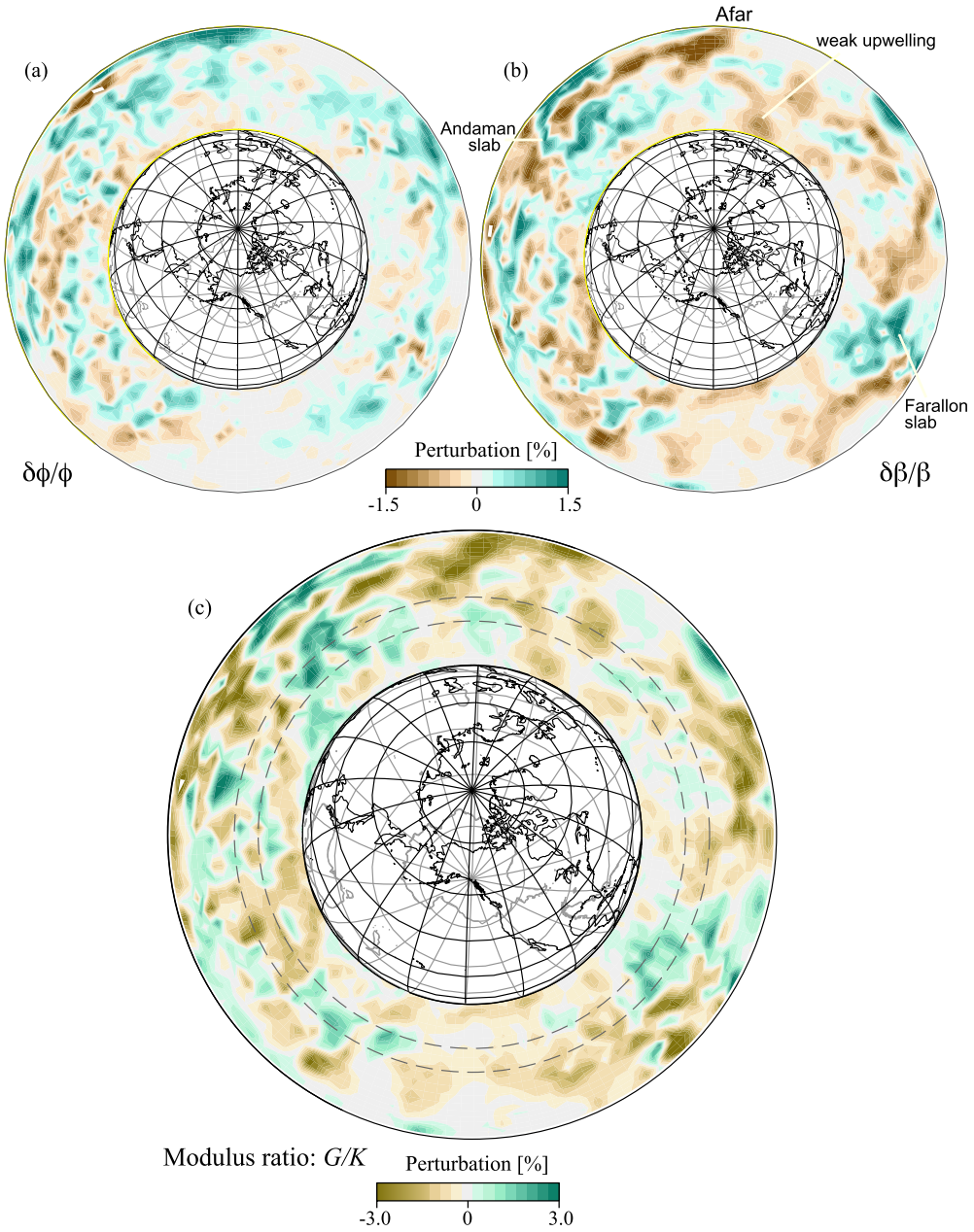

Fig. 7. A cross-section through the full globe for the joint P and S wave inversion tomographic model of Kennett and Gorbatov (2004) for (a) bulk-sound speed ϕ, (b) shear wavespeed β, and (c) the modulus ratio G/K derived from the wavespeed models. In the lower panel the dashed circles indicate depths of 1400 and 1900 km. Models are displayed as perturbations from *ak135*.

can result in such negative correlations in lower mantle properties without invoking compositional variations.

As an illustration of the actual pattern of 3-D variations, we display in Fig. 7 cross-sections of the entire globe that pass through a range of different mantle features. The plane of section cuts through the northern part of South America and passes obliquely through the high shear wavespeed zone that has been associated with past Farallon plate subduction producing a broad zone of higher wavespeeds. A more distinct subduction feature occurs on the other side of the globe, where the Andaman extension of the Indonesian subduction zone is cut directly. A narrow zone of faster wavespeeds descends to about 900 km depth. At the top of Fig. 7(b), a prominent low-velocity zone for S reaches the surface at the Afar region. This zone appears to have a weak connection to a deep zone of lowered wavespeed beneath central Africa. Possible upwelling from the core-mantle boundary can also be seen beneath the western Pacific. The blank zone in the eastern Pacific is a reflection of the limitations of the arrival-time dataset. Structure cannot be imaged unless crossing ray paths traverse the region.

A notable feature of Fig. 7 is that bulk-sound speed variations (associated with changes in bulk modulus) are relatively subdued compared to those for shear wavespeed, in part because there is little expression of subduction. This means that the image for the modulus ratio, Fig. 7(c), has a strong influence from shear. In the zone around the transition in the R_m behaviour in Fig. 5 indicated by dashed circles in Fig. 7(c), the global correlation between the variations of ϕ and β is at its weakest – slightly negative, as can be seen from Fig. 6(b). The zone of transition in the variations in modulus ratio R_m also does not display any large organised patterns in wavespeed variation, but rather smaller features of varying sign.

Tomographic methods are much more effective at imaging zones of elevated wavespeed than wavespeed reductions. This arises from the effects of wavefront healing (Malcolm and Trampert, 2011) whereby energy travelling on faster paths and diffractions tend to fill in the indent in a wavefront produced by passage through reduced wavespeeds. Large patches of lowered wavespeed survive, but smaller ones can be underestimated or even suppressed. The relatively short-scales of variation in the wavespeeds mean that such healing effects could have reduced the apparent velocity reductions.

Much of the tomographic signal for shear wavespeeds will come from temperature effects, since temperature derivatives are strong. However, the influence of temperature does not seem to be operating in the same way for bulk-sound speed. The short spatial scales of variation in the zone of transition in R_m are likely to juxtapose patches with subtly different aspects of the spin transition so that there is no large-scale coherent signal that might have a strong influence on the radial profile. Instead a muted averaged response appears to have left a faint, but distinct imprint.

The complexities of three-dimensional sampling mean that the signatures of the spin crossover in lower mantle minerals are muted. This explains the apparent seismological indifference to the spin transition (Cammarano et al., 2010; Caracas et al., 2010) without having to invoke major changes in dynamic state or issues with the quality of mineralogical predictions (Lin et al., 2018; Kurnosov et al., 2018). Only by exploiting the joint behaviour of shear and bulk modulus has it been possible to indicate the resulting weak effect.

The present work highlights the need to take into account the full set of assumptions built into seismological models (both explicit and implicit) when comparisons are made with mineral physics results.

CRediT authorship contribution statement

Brian Kennett: Conceptualization, Data analysis, Visualisation, Investigation, Writing – reviewing & editing.

Declaration of competing interest

The authors declare that they have no known competing financial interests or personal relationships that could have appeared to influence the work reported in this paper.

Acknowledgements

The constructive criticisms of two anonymous reviewers have helped refine the concepts developed in this paper. I am grateful to Steeve Gréaux, for providing the elastic modulus results used in Fig. 1, and Gaurav Shukla and Renata Wentzcovitch for the ab initio results used in Fig. 4. Emeritus support was kindly provided by the Research School of Earth Sciences of The Australian National University.

References

Antonangeli, D., Siebert, J., Aracne, C.M., Farber, D.L., Bosak, A., Hoesch, M., Krisch, M., Ryerson, F.J., Fiquet, G., Badro, J., 2011. Spin crossover in ferropericlase at high pressure: a seismologically transparent transition? Science 331, 64–67.

Badro, J., 2014. Spin transitions in mantle minerals. Annu. Rev. Earth Planet. Sci. 42, 231–248.

Boehler, R., 2000. High-pressure experiments and the phase diagram of lower mantle and core materials. Rev. Geophys. 38, 221–245.

Brown, J.M., Shankland, T.J., 1981. Thermodynamic parameters in the Earth as determined from seismic profiles. Geophys. J. Int. 66, 579–596.

Burakovsky, L., Preston, D.L., Wang, Y., 2004. Cold shear modulus and Grüneisen parameter at all densities. Solid State Commun. 132, 151–156.

Cammarano, F., Marquardt, H., Speziale, S., Tackley, P.J., 2010. Role of iron-spin transition in ferropericlase on seismic interpretation: a broad thermochemical transition in the mid mantle? Geophys. Res. Lett. 37, L03308. https://doi.org/10.1029/2009GL041583.

Caracas, R., Mainprice, D., Thomas, C., 2010. Is the spin transition in Fe^2-bearing perovskite visible in seismology? Geophys. Res. Lett. 37, L13309. https://doi.org/10.1029/2010GL043320.

Cobden, L., Goes, S., Ravenna, M., Styles, E., Cammarano, F., Gallagher, K., Connolly, J.A.D., 2009. Thermochemical interpretation of 1-D seismic data for the lower mantle: the significance of nonadiabatic thermal gradients and compositional heterogeneity. J. Geophys. Res. 114, B11309. https://doi.org/10.1029/2008JB006262.

Crowhurst, J.C., Brown, J.M., Goncharov, A.F., Jacobsen, S.D., 2008. Elasticity of (Mg, Fe)O through the spin transition of iron in the lower mantle. Science 319, 451–453.

Dziewonski, A.M., Anderson, D.L., 1981. Preliminary reference Earth model. Phys. Earth Planet. Inter. 25, 297–356.

Falzone, A.J., Stacey, F.D., 1980. Second order elasticity theory: explanation for the high Poisson's ratio of the inner core. Phys. Earth Planet. Inter. 21, 371–377.

Fu, S., Yang, J., Zhang, Y., Okuchi, T., McCammon, C., Kim, H.-I., Lee, S.K., Lin, J.-F., 2018. Abnormal elasticity of Fe-bearing bridgmanite in the Earth's lower mantle. Geophys. Res. Lett. 45, 4725–4732.

Gréaux, S., Irifune, T., Higo, Y., Tange, Y., Arimoto, T., Liu, Z., Yamada, A., 2019. Sound velocity of $CaSiO_3$ perovskite suggests the presence of basaltic crust in the Earth's lower mantle. Nature 565, 218–221.

Holmström, E., Stixrude, L., 2015. Spin crossover in ferropericlase from first-principles molecular dynamics. Phys. Rev. Lett. 114 (11), 117202.

Houser, C., Hernlund, J.W., Valencia-Cardona, J., Wentzcovitch, R.M., 2020. Discriminating lower mantle composition. Phys. Earth Planet. Inter. 308, 106552.

Irifune, T., Shinmei, T., McCammon, C.A., Miyajima, N., Rubie, D.C., Frost, D.J., 2010. Iron partitioning and density changes of pyrolite in Earth's lower mantle. Science 327, 193–195.

Kaneshima, S., Helffrich, G., 2013. Vp structure of the outermost core derived from analysing large-scale array data of SmKS waves. Geophys. J. Int. 193, 1537–1555.

Kennett, B.L.N., 1998. On the density distribution within the Earth. Geophys. J. Int. 132, 374–382.

Kennett, B.L.N., 2017. Towards constitutive equations for the deep Earth. Phys. Earth Planet. Inter. 270, 40–45.

Kennett, B.L.N., 2020a. Radial Earth models revisited. Geophys. J. Int. 222, 2189–2204.

Kennett, B.L.N., 2020b. Towards constitutive equations for the deep Earth II: shear properties under pressure. Phys. Earth Planet. Inter. 307, 106558.

Kennett, B.L.N., Engdahl, E.R., Buland, R., 1995. Constraints on seismic velocities in the Earth from travel times. Geophys. J. Int. 122, 108–124.

Kennett, B.L.N., Gorbatov, A., 2004. Seismic heterogeneity in the mantle - strong shear wave signature of slabs. Phys. Earth Planet. Inter. 146, 88–100.

Kurnosov, A., Marquardt, H., Frost, D.J., Ballaran, T.B., Ziberna, L., 2018. Kurnosov et al. reply. In: Communications Arising. Nature 564 (7736), E27–E31.

Lin, J.-F., Vanko, G., Jacobsen, S.D., Iota, V., Struzhkin, V.V., Prakapenka, V.B., Kuznetsov, A., Yoo, C.-S., 2007. Spin transition zone in Earth's lower mantle. Science 317, 1740–1743.

Lin, J.-F., Speziale, S., Mao, Z., Marquardt, H., 2013. Effects of the electronic spin transitions of iron in lower mantle minerals: implications for deep mantle geophysics and geochemistry. Rev. Geophys. 51, 244–275.

Lin, J.F., Mao, Z., Yang, J., Fu, S., 2018. Elasticity of the lower-mantle bridgmanite. In: Communications Arising. Nature 564 (7736), E18–E26.

Liu, J., Dorfman, S.M., Zhu, F., Li, J., Wang, Y., Zhang, D., Xiao, Y., Bi, W., Alp, E.E., 2018. Valence and spin states of iron are invisible in Earth's lower mantle. Nat. Commun. 9, 1284. https://doi.org/10.1038/s41467-018-03671-5.

Mao, Z., Lin, J.F., Liu, J., Prakapenka, V.B., 2011. Thermal equation of state of lower-mantle ferropericlase across the spin crossover. Geophys. Res. Lett. 38, L23308. https://doi.org/10.1029/2011GL049915.

Marquardt, H., Speziale, S., Reichmann, H.J., Frost, D.J., Schilling, F.R., 2009. Single-crystal elasticity of $(Mg_{0.9}Fe_{0.1})O$ to 81 GPa. Earth Planet. Sci. Lett. 287, 345–352.

Malcolm, A.E., Trampert, J., 2011. Tomographic errors from wave front healing: more than just a fast bias. Geophys. J. Int. 185, 385–402.

Marquardt, H., Buchen, J., Mendez, A.S.J., Kurnosov, A., Wendt, M., Rothkirch, A., Pennicard, D., Liermann, H.-P., 2018. Elastic softening of $(Mg_{0.8}Fe_{0.2})O$ ferropericlase across the iron spin crossover measured at seismic frequencies. Geophys. Res. Lett. 45, 6862–6868.

Marquardt, H., Thomson, A.R., 2020. Experimental elasticity of Earth's deep mantle. Nat. Rev. Earth & Environ. 1 (9), 455–469.

Montagner, J.-P., Kennett, B.L.N., 1996. How to reconcile body-wave and normal-mode reference Earth models? Geophys. J. Int. 125, 229–248.

Piet, H., Badro, J., Nabiei, F., Dennenwaldt, T., Shim, S.-H., Cantoni, M., Hébert, C., Gillet, P., 2016. Spin and valence dependence of iron partitioning in Earth's deep mantle. Proc. Natl. Acad. Sci. 113, 11 127–11 130.

Saltzer, R., van der Hilst, R.D., Karáson, H., 2001. Comparing P and S wave heterogeneity in the mantle. Geophys. Res. Lett. 28, 1335–1338.

Shukla, G., Cococcioni, M., Wentzcovitch, R.M., 2016. Thermoelasticity of Fe^{3+}- and Al-bearing bridgmanite: effects of iron spin crossover. Geophys. Res. Lett. 43, 5661–5670.

Simmons, N.A., Forte, A.M., Boschi, L., Grand, S.P., 2010. GyPSuM: a joint tomographic model of mantle density and seismic wave speeds. J. Geophys. Res. 115, B12310. https://doi.org/10.1029/2010JB007631.

Speziale, S., Milner, A., Lee, V.E., Clark, S.M., Pasternak, M.P., Jeanloz, R., 2005. Iron spin transition in Earth's mantle. Proc. Natl. Acad. Sci. 102, 17 918–17 922.

Tsuchiya, T., Wentzcovitch, R.M., da Silva, C.R.S., de Gironcoli, S., 2006. Spin transition in magnesiowüstite in Earth's lower mantle. Phys. Rev. Lett. 96 (19), 198 501–198 504.

Valencia-Cardona, J.J., Williams, Q., Shukla, G., Wentzcovitch, R.M., 2017. Bullen's parameter as a seismic observable for spin crossovers in the lower mantle. Geophys. Res. Lett. 44, 9314–9320.

Wentzcovitch, R.M., Justo, J.F., Wu, Z., da Silva, C.R.S., Yuen, D.A., Kohlstedt, D., 2009. Anomalous compressibility of ferropericlase throughout the iron spin cross-over. Proc. Natl. Acad. Sci. 106 (21), 8447–8452.

Wu, Z., 2016. Velocity structure and composition of the lower mantle with spin crossover in ferropericlase. J. Geophys. Res., Solid Earth 121 (4), 2304–2314.

Wu, Z., Justo, J., Wentzcovitch, R., 2013. Elastic anomalies in a spin-crossover system: ferropericlase at lower mantle conditions. Phys. Rev. Lett. 110, 228501.

Wu, Z., Wentzcovitch, R.M., 2014. Spin crossover in ferropericlase and velocity heterogeneities in the lower mantle. Proc. Natl. Acad. Sci. 111, 10 468–10 472.

Wu, Z., Wentzcovitch, R.M., 2017. Composition versus temperature induced velocity heterogeneities in a pyrolitic lower mantle. Earth Planet. Sci. Lett. 457, 359–365.